Evaluation of an air spinning process to produce tailored biosynthetic nanofiber scaffolds

Marie Gad Sabbatier[1,2,3], Pierre Abadie[2,3], Florence Dieval[1], Bernard Durand[1] and Gaétan Laroche[2,3]

[1]*Laboratoire de Physique et Mécanique Textile, École Nationale Supérieure d'Ingénieurs du Sud Alsace, Université de Haute Alsace, 11 rue Alfred Werner - 68093 Mulhouse Cedex, Mulhouse, France.*
[2]*Laboratoire d'Ingenierie de Surface, Centre de Recherche sur les Materiaux Avancés, Département de génie de mines, de la métallurgie et des matériaux, Université Laval 1045 avenue de la Medecine.*
[3] *Centre de recherche du CHU de Québec. Hôpital St Francois d'Assise, 10, rue de L'Espinay, local E0-165, Québec (QC), G1L 3L5 Québec, Canada*

ABSTRACT
We optimized the working parameters of an innovative air spinning device to produce nanofibrous polymer scaffolds for tissue engineering applications. Scanning electron microscopy was performed on the fiber scaffolds which were then used to identify various scaffold morphologies based on the ratio of surface occupied by the polymer fibers on that covered by the entire polymer scaffold assembly. Scaffolds were then produced with the spinning experimental parameters, resulting in 90% of fibers in the overall polymer construct, and were subsequently used to perform a multiple linear regression analysis to highlight the relationship between nanofiber diameter and the air spinning parameters. Polymer solution concentration was deemed as the most significant parameter to control fiber diameter during the spinning process, despite interactions between experimental parameters. Based on these findings, viscosity measurements were performed to clarify the effect of the polymer solution property on scaffold morphology.

1   INTRODUCTION

In the most serious cases of vascular disease, surgeons have no choice but to replace the arteries with vascular prostheses [1, 2] which are manufactured in either woven or knitted polyethylene terephthalate (PET) or microporous expanded polytetrafluoroethylene (ePTFE) and are used to replace arteries with a diameter greater than 6 mm. For smaller diameters, no long-term solution exists for artery replacement [3], primarily because these materials are highly thrombogenic. Indeed, when the surface of the material is in contact with blood, coagulation factors are activated which

leads to blood clot formation [4]. This foreign-body reaction [5] can be avoided that the prosthesis is able to accommodate an endothelial cell monolayer that resembles the inner surface of the artery.

Our previous studies have demonstrated the ineffectiveness of endothelial cell monolayer growth on the textile structure of prostheses due to a dimensional mismatch between prosthesis structure scale and cell size [6]. Our strategy is to bridge this mismatch by coating the internal surface of the prosthetic tube with a polymeric nanofiber scaffold to produce a temporary synthetic extracellular matrix [7]. In addition to making it possible for endothelial cells to adhere and proliferate, this coating helps preserve the mechanical properties of the prosthesis.

Choosing the right polymer for this coating is crucial [8]. The polymer must be biocompatible and easy to produce. In this regard, high molecular weight poly(lactic acid) (PLA) is an ideal candidate, as medical devices made with this polymer are approved by the Food and Drug Administration[9] and is commonly deployed in medical and paramedical applications. Used as suture thread for many years [10], PLA was recently shown to provide an alternative to permanent stents [11, 12], and it is also a suitable polymer for drug delivery applications [13] due to its biodegradation features. This aliphatic polyester consists of a linear chain synthesized by the ring opening polymerization and polycondensation of the lactide dimer. Thanks to its ester-containing structure, this polymer can be degraded through hydrolysis and its degradation rate can be tailored to meet the requirements of each application [14, 15].

The most common method to produce nanofibers is the electrospinning process [16]. In this technology, a high voltage is applied between a needle and a collector to draw fibers from a solution. This easy process has been widely studied and can produce either classical or porous [17] synthetic and natural fibers. More complex morphologies have been spun, such as composite fibers [18], core-shell fibers [19], and ceramics, as well as carbon nanotubes and nanofibers [20]. The shape morphology can also be controlled to produce unidirectional and multidirectional patterns [21]. Finally, the variety of yarns and shapes provide a wide range of applications in numerous scientific fields.

Despite the definite advantages of electrospinning, this method cannot readily be used to coat the luminal surface of a tubular textile vascular prosthesis [7] because of the small distances between the needle and the surface. To address this issue, we developed an alternative device, called air spinning which involves the stretching of a polymer solution under high-speed air flow. This technique was introduced by our group in 2008 [7] and has been continuously upgraded for the coating of tubular shapes [22].

Nanofiber technology is extensively used in biomedical and tissue engineering applications [23], as well as in bone and cartilage applications [24, 25], in skin regenerative medicine [26]or cardiac tissue repair applications [27]. Nanofibers are now being formed as scaffolds to promote cell adhesion and proliferation and also differentiation [28] and guided migration [29], and their surface and physical properties are tunable to target protein adsorption [30]. In addition, natural or synthetic scaffolds can be functionalized to add biomimicry and improve bioactivity [31].

François et al. [7] showed that cell behavior depends on the quality of the air-spun nanofiber scaffold which can be determined by the number of fiber fractures, fiber diameter, and scaffold morphology. In a previous study [7], Fiber ruptures were quantified and correlated with spinning parameters, yet no information was provided as to fiber diameter and scaffold morphology with the air-spinning device. Oliveira et al. [32] characterized solution blow-spinning using a system similar to the one previously developed in our laboratory. These authors correlated blow-spinning parameters with fiber diameter but with a different set of parameter ranges. Moreover, some important parameters, such as needle diameter and substrate/needle distance were not considered.

The aim of this study was thus to further the state of knowledge regarding the air spinning process to better understand fiber formation, optimize spinning parameters for a more uniform fiber shape, and develop methods and tools to predict optimal spinning conditions.

2   MATERIALS AND METHODS

2.1   Air spinning process and parameters

PLA (Mw = 150000, Ip = 2.45, D/L = 4.5%, T_g = 61°C, Tm = 144°C, CML poly(lactic acid), Hycail Finland Oy, Turku, Finland) was totally solubilized in chloroform (99.8%, Laboratoire Mat, Québec, QC, Canada) and injected into an air spinning device (Fig.1 [7]). The PLA solutions were then stretched under high-speed air flow and pulverized on PET films that were fastened onto the collector (Goodfellow, Oakdale, PA, USA). The polymer solution residence in the air flow enabled the nanofibers to form upon solvent evaporation.

The air spinning apparatus was equipped with a flow control syringe pump (NE-1010, New Era Pump System, Farmingdale, NY, USA) and a 20 mL luer lock glass syringe containing the polymer solutions. The syringe was first mounted onto an injector equipped with a small needle (1/2" Straight Cannula Crimp Sealed, I&J Fisnar, Wayne, NJ, USA), then attached to a homemade atomizer fed with compressed medical-grade air. The nanofiber coating was homogeneously settled on the collector with X and Y computerized translation stages (Velmex, Bloomfield, NY, USA).
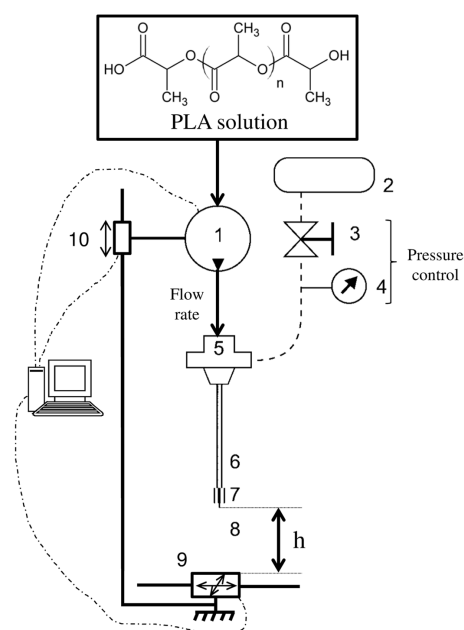

Figure 1. Air spinning system set-up. (1) syringe pump; (2) compressed air tank; (3) air valve; (4) manometer; (5) atomizer; (6) injector with small needle; (7) nozzle; (8) pulverization cone; (9) XY translation stage and collector; and (10) Z-stage.

The effect of polymer solution concentration, needle diameter, flow rate, pressure, and nozzle-to-sample distance was investigated in terms of its influence on fiber diameter, with the ranges determined either from previous studies [7] or on the basis of physical constraints. Flow rates and pressure values were set accordingly between 10 mL/h and 50 mL/h and between 5 MPa and 10 MPa, respectively, while polymer solutions were investigated at concentrations ranging between 1% and 15% to enable flow rate control in the lower diameter needle (0.15 mm) while preventing clotting in the higher diameter one. The nozzle-to-sample distance values were set at between 200mm and 300 mm, as a previous study by our group demonstrated that these lengths were sufficient to produce solvent-free polymer fibers.

2.2 Morphology study and fiber diameter measurements

Thirteen solutions of varying PLA concentrations (1, 1.5, 2, 3, 4, 5, 6, 7, 8, 9, 10, 12, and 15% w/v) were randomly air-spun with four needles of different diameters (0.6, 0.41, 0.25, and 0.15 mm). For this section of the experiment, flow rate, air pressure, and nozzle-to-sample distance (h) were kept constant at 10 mL/h, 5 MPa, and 200 mm, respectively. Each sample was duplicated, gold-coated, and subsequently observed under a scanning electron microscope (JSM840A, JEOL, Tokyo, Japan). Three images per sample were randomly taken at a magnitude of 1000 for the morphology study and either 3000 or 10000 for the fiber diameter measurements. Each image was then analyzed with image treatment software (Image J, National Institutes of Health, Bethesda, MD, USA). The ratio between the surface covered by the fibers (S_{fibers}) and the surface covered after spinning ($S_{covered}$) was then calculated.

Finally, approximately 25 fiber diameters were evaluated per image for an approximate total of 150 diameter measurements for each experiment. The measurements were compared with a Gaussian profile to determine the relevance of using the diameter average for the rest of the study, which was a condition to performing a statistical analysis.

2.3 Experimental design and statistical analysis

A least squares multiple linear regression was performed to determine the relationship between the spinning experimental parameters and the fiber diameter. This method consists in fitting an experimental parametric model with a linear mathematical model. The calculation of estimated regression parameters of this model is established by the following equation (Equation 1):

$$\hat{\underline{\beta}} = (\underline{X}^T\underline{X})^{-1}\underline{X}^T\underline{Y} \tag{1}$$

where, $\hat{\underline{\beta}}$ is the vector of the estimated regression coefficient values, $\underline{X}$ is the parameter matrix, and $\underline{Y}$ is the vector of responses.

Model robustness was then statistically evaluated [33]. First, an analysis of variance was performed to ascertain model significance. The hypothesis that at least one of the regression coefficients was significant was ascertained through the validation of Equation 2:

$$\frac{MSR}{MSE} > F((p-1);(n-p)) \tag{2}$$

where MSR is the regression mean square, MSE is the mean square error, $F((p-1);(n-p))$ is the F-test value, p is the number of parameters, and n is the number of experiments. The F-test was performed with a level of confidence of 5%.

Thereafter, the statistically non-significant parameters were rejected with a confidence interval analysis on the estimated regression coefficient values. The confidence interval was calculated by $\hat{\beta}_i \pm t_{\frac{\alpha}{2},n-p}\sqrt{C_{ii} \times MSE}$, where $\hat{\beta}_i$ is the regression coefficient value for parameter i, C_{ii} is the diagonal value of $\underline{C} = (\underline{X}^T\underline{X})^{-1}$ for parameter i, and $t_{\frac{\alpha}{2},n-p}$ represents the t-test value for a confidence interval of α. Parameters leading to a confidence interval less than 5% were rejected from the model.

Finally, three models were normalized and compared to identify the most accurate one. The first (M1) and second models (M2) consisted of working on two-level interactions which consisted of 32 experiments. Eight experiments were added to test a quadrature model (Table 1b), which resulted in a third model (M3).

Table 1. Experimental designs

Variables	Parameters	2⁵ Factorial experiment design values (a)		Added values (b)	
		X-	X+	X-	X+
X_C	Concentration (%w/v)	4	10	7	7
X_D	Needle diameter (mm)	0.25	0.41	0.25	0.41
X_P	Air pressure (MPa)	5	10	5	10
X_F	Flow rate (mL/h)	10	50	10	50
X_h	Distance h (mm)	200	300	200	200

2.4 Viscosity measurements

Statistical analyses highlighted the effect of the solution properties and consequently, PLA solution viscosity was measured by means of a shear stress rheometer (ARES-G2, TA Instruments, New Castle, DE, USA) at 25°C at an imposed shear stress speed ranging between 1 s^{-1} and 1000 s^{-1}. A standard 2°-cone and plate geometry with a 60 mm diameter was used to apply the shear stress. Viscosity was established for PLA solutions at various concentrations in the permanent regime. Because the dynamic viscosity remained constant, each solution was considered as a Newtonian fluid (results not shown) on the scale. Each viscosity measurement was made over a period of approximately 600 s. However, the polymer solution viscosity data reported therein were measured at the very beginning of the experiments, therefore preventing any increase of polymer viscosity due to solvent evaporation. Specific viscosity of the PLA was then calculated to eliminate the solvent effect using the following equation (Equation 3):

$$\vartheta_{sp} = \frac{\vartheta_{dyn} - \vartheta_{solvent}}{\vartheta_{solvent}} \tag{3}$$

where ϑ_{sp} is the specific viscosity, ϑ_{dyn} is the dynamic viscosity of the solution (in Pa.s) chloroform, and $\vartheta_{solvent}$ is the viscosity of chloroform (in Pa.s).

The polymer solution regimes were highlighted with power profiles of specific viscosity, as a function of concentration, and the best fitted curves were retained.

3 RESULTS AND DISCUSSION

3.1 Morphology study

For the sake of discussion, spinnability regimes are considered to be those during which PLA nanofibers can be obtained, regardless of the formation of beads or puddles. The puddles in our experiment were defined by macroscopic elements inside the scaffold that were easily visible to the naked eye. Figures 2a, 2b, and 2c present typical images of the air-spun PLA polymer solutions. Figures 2a and 2c display the so-called beads and puddles, respectively, which constituted

undesired elements for the targeted biomedical application and were the result of two different instabilities during the spinning process (see discussion section).
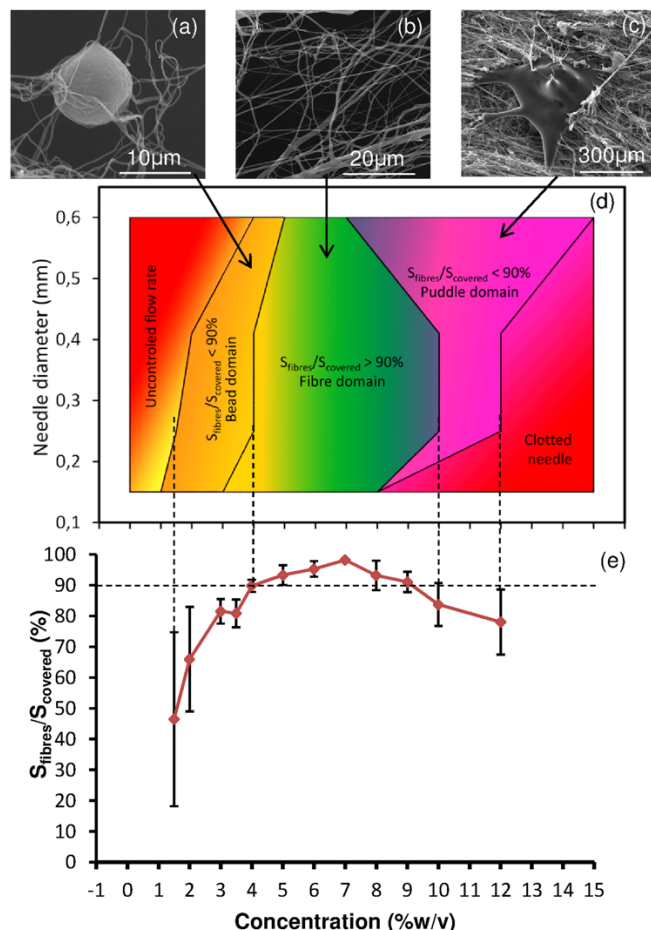

Figure 2. Air spun nanofiber scaffold morphologies. (a) bead inside the scaffold; (b) nanofiber scaffold; (c) puddle of PLA polymer; (d) functioning chart, (e) surface ratio using a 0.25 mm-diameter needle.

Figure 2e provides an example for a needle of 0.25 mm and shows the evolution of surface ratio ($S_{fibers}/S_{covered}$) of the fibers, which covered the samples, as a function of PLA concentration. As shown in this figure, the spinnability concentration ranged between 1.5 and 12% w/v. Samples with a surface ratio up to 90% were defined as a fiber domain. In practice, this definition applies to concentrations between 4 and 10% w/v, which basically corresponds to the plateau region in Figure 2e. These samples were reproducible and uniform, as observed through the relative fiber to (bead/puddle) surface ratio ($S_{fibers}/S_{covered}$) measurement error bars. The best reproducibility result was achieved with a 7% PLA concentration, which also turned out to be the conditions at which a bead- or puddle-free fiber network was achieved. Samples with a surface ratio of less than 90% were defined as either a bead or puddle domain where these elements were more numerous. SEM observations showed that puddles did appear with higher concentrations and are presented while the surface ratio decreased with concentrations inferior to 90%.

These measurements were also performed with needle diameters of 0.6, 0.41, and 0.15 mm. Comparing these results with those presented in Figures 2a-c enabled us to determine an overall PLA fiber formation behavior, as depicted in Figure 2d. Of interest is that fiber formation with the lowest concentration occurred at 1.5% w/v for a needle diameter of 0.15 mm, while beads only

appeared at 1% w/v for this needle diameter. On one hand, solution flow was uncontrolled for the lowest concentration and highest needle diameter. On the other hand, the PLA solutions in the highest concentration range were too viscous to flow with ease through the lowest needle diameters.

Based on the data presented in Figure 2, we then focused on examining the experimental concentrations between 4 and 10% w/v with 0.41 and 0.25 mm-diameter needles, as this set of ranges produced the highest fiber-to-bead/puddle ratio.

3.2 Diameter measurements

Figure 3 presents the distribution of nanofiber diameters for X_C = 4% w/v, X_D = 0.25 mm, X_P = 5 MPa, X_F = 10 mL/h and X_h = 200 mm.
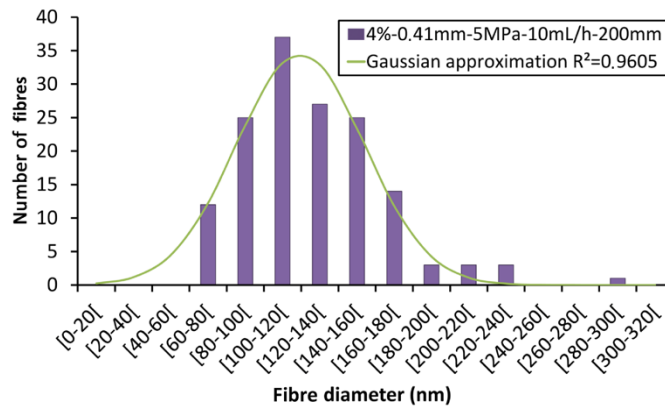

Figure 3. Typical distribution of nanofiber diameter.

In order to perform statistical analyses, the data presented in Figure 3 were fitted using a Gaussian profile [32, 34, 35]. As depicted in this figure, this choice was justified by the excellent correlation coefficient between the experimental data and the fitted Gaussian curve, which greatly simplified the statistical analyses.

An identical analysis was performed for the entire set of experiments presented in Table 1 (results not shown). Correlation factors calculated from the Gaussian fit were relatively high (more than 0.7) for all of the experiments, and consequently, an average of the nanofiber diameter values could be used to estimate the Y values for the entire set of experimental designs.

3.3 Experimental designs

Three models were established from the data presented in Table 1. The first and second models were calculated from the values in Table 1a. Experiments from Table 1b were added to constitute the third model. An analysis of variance revealed a significant group effect on the nanofiber diameter for the three models (M1: α = .05, $F_{(4,27)}$ < 178, p < .001; M2 : α = .05, $F_{(14,18)}$ < 136.96, p < .001; M3 : α = .05, $F_{(15,25)}$ < 73.1, p < .001). Figure 4 presents the results of the least squares multiple regressions.

Model 1

$$Y = 365.8 + 237.0X_C - 26.6X_D \ (4)$$

$$R^2 = 0.9716$$

Linear coefficients

β0 β1 β2 β3 β4 β5

Model 2

$$Y = 365.8 + 363.7X_C - 129.3X_{CD}$$
$$-59.5X_{CP} - 59.3X_{DF} \ (5)$$

$$R^2 = 0.9923$$

Linear coefficients   Interaction coefficients

β0 β1 β2 β3 β4 β5 β12 β13 β14 β15 β23 β24 β25 β34 β35 β45

Model 3

$$Y = 378.8 + 580.2X_C - 118.6X_{CD}$$
$$-55.3X_{CP} - 257.2X_C^2 \ (6)$$

$$R^2 = 0.9846$$

Linear coefficients   Interaction coefficients   Quadrature coefficient

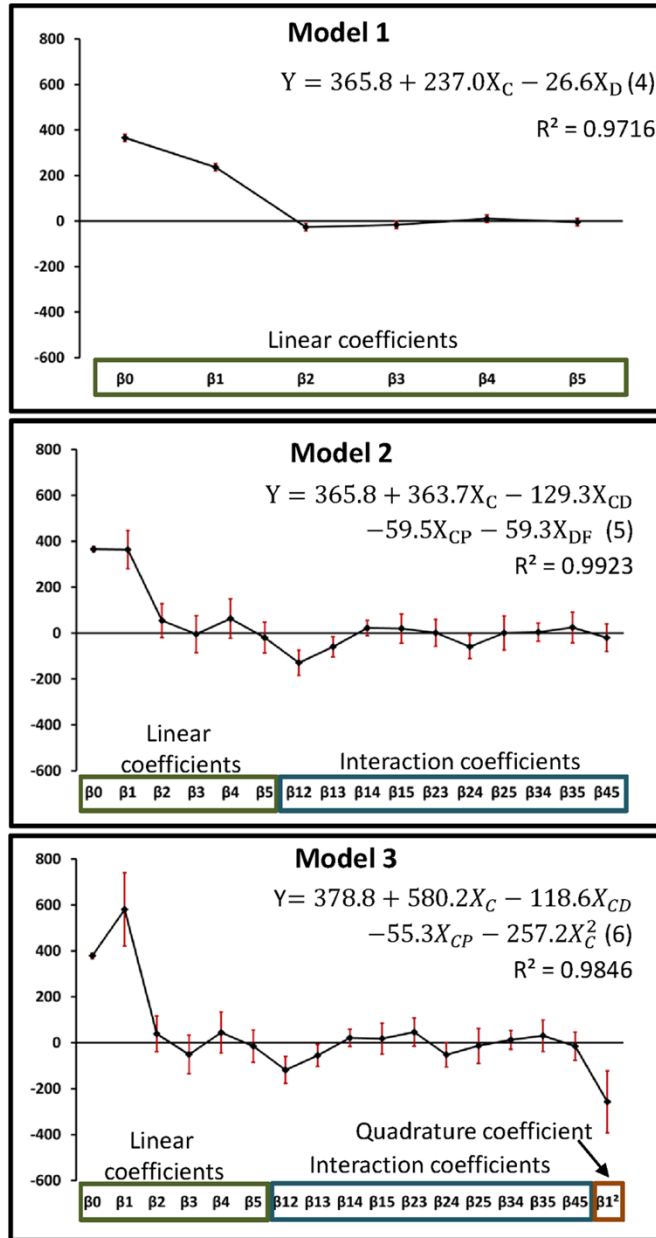β0 β1 β2 β3 β4 β5 β12 β13 β14 β15 β23 β24 β25 β34 β35 β45 β1²

Figure 4. Confidence intervals for regression coefficients and model equations (XC: solution concentration, XD: needle diameter, XF: flow rate, XP: pressure, a X coefficient with two subscript letters indicates an interaction between two parameters (e.g., XCD = XC.XD)).

All possible cases were calculated, from single interaction to saturated models, which enabled us to determine the more significant parameters used thereafter to build up models 1, 2, and 3.

In our initial observation, PLA solution concentration (XC) was clearly the most significant parameter considering all three models (Equations 4, 5, and 6), and the only one to lead to an increase in nanofiber diameter (positive sign), as shown in Figure 4. Needle diameter (XD), air pressure (XP), and solution flow rate (XF), although less significant, also had to be taken into account, as they appeared in interaction terms. Finally, the distance between the needle and the substrate (Xh) had clearly no effect on fiber diameter, which signifies, from a physical standpoint, that all of the solvent had evaporated during spinning for the investigated needle-to-sample distance.

Model 1 (Equation 4) served as a basis for comparison by taking into account that no interaction existed between the various investigated parameters. Accordingly, in the first approximation, this model demonstrated that polymer concentration and needle diameter were both significant parameters in controlling PLA nanofiber diameter.

Although not perfect, Model 1 allowed for the anticipation of parameters which could potentially interact with other set-up condition parameters, such as concentration, and to a lesser extent, needle diameter. Superior correlation coefficients were thus obtained in Model 2 (Equation 5) and Model 3 (Equation 6), while considering the interaction of pressure and concentration (XCP) and were therefore more in line with the assumption that air pressure should somehow play a role in the air-spun PLA fiber diameter. Model 2 showed that the needle diameter parameter was significant only when considering its interaction with concentration and flow rate.

Model 3 was also constructed from first-hand information obtained from Model 1. Indeed, the singular importance of PLA concentration demonstrated in Model 1 led to the logical integration of a quadrature concentration term which was shown, however, not to bring as much precision to the model. Indeed, despite being rather high, the regression coefficient calculated with Model 3 remained lower than that with Model 2, which confirms that the quadrature coefficient factor had little significance in terms of controlling air-spun PLA fiber diameter. Similarly, the interaction between needle diameter and flow rate became insignificant due to the addition of experimental data to build up Model 3. Thus, the control of PLA nanofiber diameter through air spinning was better described by Model 2.

3.4. Viscosity results

The importance of the concentration parameter on the PLA nanofiber diameter highlighted above may be extended to a larger concentration range to further explain the so-called formation of polymer beads (at concentrations lower than that of the fiber formation concentration domain) and polymer puddles (higher than that of the fiber formation concentration domain). However, this can be more easily conceptualized by considering the polymer specific viscosity calculated in Equation 2 which is known to be concentration dependent, as is clearly evidenced in Figure 5.
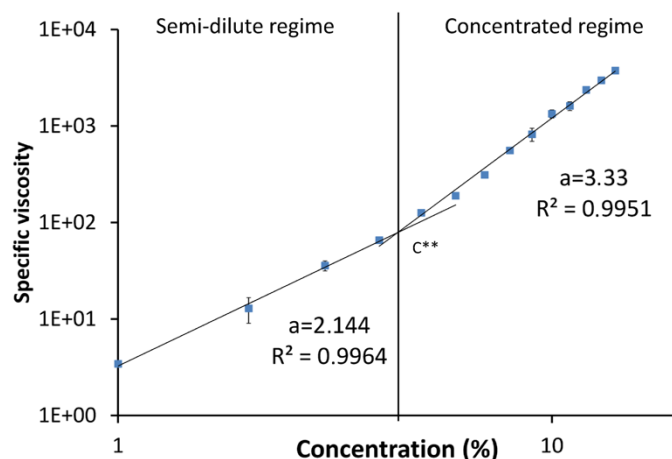

Figure 5. Specific viscosity of PLA solutions as a function of polymer concentration.

Figure 5 shows two different regimes, with each one playing a key role in the extension of the polymer chains inside the solution and ultimately contributing to nanofiber formation and integrity. The first region produced concentration values between 1% w/v and C** (approximately 4.3% w/v) [36-38] and thus represented the semi-dilute regime. C** was the critical concentration between low-interacting polymer chains (where movements between chains were possible) and a state where the

chains were totally entangled. In the semi-dilute state, the solvent surrounded the polymer chains, forming blobs and leading to few molecular interactions between the polymer molecules. In the concentrated regime, the polymer chains were significantly entangled [36]. Air spinning of PLA in the semi-dilute regime led to an elevated concentration of the so-called beads within the polymer fiber network, whereas in the concentrated regime, nanofiber formation was definitely stabilized. Of note, the curve slopes presented in Figure 5 correlate with those in previously published research [36, 39].

4   DISCUSSION

Our research group developed an alternative and innovative method for the spinning of nanofibers to coat vascular prostheses which is impossible with a conventional electrospinning device [22]. We also demonstrated the biocompatibility of PLA air-spun nanofiber scaffolds with endothelial cells [7].

In this study, optimization of the nanofiber assembly was achieved by quantifying the quality of spinning by calculating fiber surface coverage and diameter. Our results enabled us to determine a range of concentration to produce a maximized nanofiber quality (4% w/v-10% w/v). The data show that optimum scaffold quality was achieved with approximately 7% w/v concentration using either 0.25 or 0.41 mm-diameter needles. These values are obviously difficult to directly compare with those of electrospinning because of the different stretching forces (electric fields as opposed to air flow)[40-42] and polymer solution characteristics involved [16]. It should also be emphasized that similar spinning procedures may lead to different fiber diameters and scaffold morphologies due to differences in design set-up.

As shown in Figure 2, the experimental parameter limits of the air-spun apparatus were determined to produce the most appropriate fibrous scaffold for tissue engineering applications. A fiber scaffold was defined as containing more than 90% of polymer fibers, as determined by measuring the surface ratio of the area occupied by the polymer fibers on that of the overall polymer assembly (including fibers, puddles, and beads).

Beads are usually shown as a defect in the electrospun nanofiber domain due to the Rayleigh-Plateau instability [43] and have been known to have a negative influence on mechanical properties [44]. Indeed, uniform fibers lead to a continuous traction stress state. On the contrary, the presence of beads may create local traction stress concentration and ultimately lead to early failure.

As for the biological considerations, one objective in using a nanofiber scaffold is to mimic the extracellular matrix for cell adhesion and proliferation. The presence of polymer beads within the scaffold structure must therefore be minimized accordingly. Under optimal conditions (concentration 7%, needle diameter 0.25 mm), beads occupy a surface area of close to 3% of the overall fiber assembly, with minimal impact to the scaffold's mechanical properties.

To our knowledge, our study is the first to report the formation of puddles in a fiber spinning process. Our data indicate that these features are likely due to instabilities (different from those responsible for bead formation) and occur at high polymer solution concentrations (greater than 9-10% w/v with a needle diameter of 0.25 mm). In electrospinning, high polymer concentrations result in the disappearance of beads [45], contrary to what is observed in air spinning in which high polymer concentration solutions are apparently too viscous to be stretched by high speed air flow, thereby preventing efficient solvent evaporation and leading to the formation of the so-called puddles instead of nanofibers. A solution to this problem may be to considerably increase air pressure which, however, may cause deleterious fiber failure and subsequent early degradation upon utilization as a biological scaffold [7]. Moreover, the aforementioned puddles formed at high polymer concentrations are likely to contain residual solvent which may ultimately be toxic for cells.

The parameters presented in Table 1 are typically chosen in research [16, 35, 38, 45, 46] to study spinning devices and are known to have a significant effect on fiber morphology. Within the parameter ranges, the spun fibers had a diameter close to 100 nm. Consequently, nanofiber

scaffolds produced in this range of parameters will not only bridge the dimensional mismatch between PET textile microfibers or microporous ePTFE structures of vascular prostheses and endothelial cell dimensions [6, 7], but also lead to monolayer cell proliferation. Our prototype therefore meets the requirements of matching the mechanical properties of PET vascular prostheses while adapting endothelial cell proliferation in a monolayer.

The biodegradable nature of PLA must also be taken into account in the design of a scaffold for biomedical applications. During completion of the cell adhesion, proliferation confluence, and maturation processes, it is expected that the nanofiber scaffold be progressively replaced by the natural extracellular matrix [47]. Consequently, intrinsic material properties and scaffold morphology must be controlled to hone the PLA degradation kinetics. Indeed, fiber diameter has direct consequences on degradation rate[48]. In this regard, determining nanofiber diameter also provides additional information on the degradation control mechanism related to scaffold morphology.

Robust multilinear regression models were used to describe nanofiber diameter distribution as a function of the air spinning experimental parameters. Although Model 1 (no interaction between parameters) was shown to produce less accurate information, it did, however, provide a better understanding of parameter significance and interaction origin. From this model, PLA solution concentration was clearly shown to be the most significant parameter in controlling nanofiber diameter. This first-hand information also enabled us to construct more precise models that considered giving greater importance to the concentration parameter (Model 3) or to the interactions between polymer solution concentration and other spinning parameters (Model 2).

Model 2 provided us with the best correlation coefficient, therefore highlighting the overall importance of controlling each and every parameter of the spinning procedure. Moreover, it supports the assumption that some driving forces related to the interactions between such experimental parameters as polymer solution concentration, needle diameter, air pressure, and polymer solution flow rate, may influence the spinning process. For example, the interaction between PLA solution concentration and needle diameter (XCD) was directly linked to the surface tension of the drop at the needle tip [47, 49, 50] and therefore controlled the drop size and the quantity of solution which was instantaneously stretched. Similarly, mechanical forces deployed to stretch the fibers were related to the interaction between PLA concentration and air pressure (XCP). This is in agreement with the results presented in Figures 2a-c which showed that high-viscosity polymer solutions were harder to stretch.

PLA solution concentration is the most difficult parameter to ascertain. In fact, this study demonstrates that it is the viscosity of the polymer solution (which in turn depends on such parameters as stereochemistry [42], copolymerization [47], molecular weight [51], and concentration) which must be taken into account to control fiber diameter and scaffold morphology. In this context, the polymer solution concentration must only be considered as an indicator of the more global parameter, namely, viscosity. Figure 5 shows two different dilution regimes depending on the concentration. These results correlate with those presented in Figures 1 and 2 which show three spinning domains. Essentially, bead domain ($S_{fibers}/S_{covered}$ < 90%) was observed in the semi-dilute regime while fiber domain was observed in the concentrated regime ($S_{fibers}/S_{covered}$ > 90%). When polymer concentration increased above 10%w/v, (needle diameter 0.25 mm), the solution viscosity was simply too high to stretch the polymer assembly. This confirms that the precise location of the borders between domains is needle diameter-dependent.

These results demonstrate that low-viscosity polymer solutions lead to the occurrence of bead formation [52, 53]. This can be explained by the fact that some polymer molecules in the semi-dilute regime were isolated, resulting in bead formation, while others were more entangled, which ultimately promoted fiber network development. In the concentrated regime, the polymer chains were highly entangled which, along with experimental parameters such as the small needle diameter of the injector and the relative low air pressure, promoted further contact between the polymer chains. This interpretation has been shown to theoretically predict the fiber [54].

Overall, fiber scaffold formation by the air spinning method is somewhat similar to that produced by electrospinning in terms of its polymer solution viscosity dependence, which therefore signifies that both spinning techniques require polymers with molecular weights that are high enough to attain the concentrated domain.

5 CONCLUSIONS

In this study, we optimized the experimental parameters of an innovative spinning process developed to coat vascular prostheses with a PLA scaffold to promote endothelial cell adhesion and proliferation. Bead, fiber, and puddle domains were evident for various needle diameters and polymer concentrations. Our data demonstrate that an optimal fiber scaffold is achievable with a polymer concentration of approximately 7% w/v and a needle diameter of 0.25 mm. Multilinear regression was performed to develop models to establish the relationship between fiber diameter and the various spinning parameters and confirms the paramount importance of the polymer solution concentration. Viscosity measurements were also conducted to highlight the physical aspects of fiber formation.

REFERENCES

[1] A.T. Hirsch, Z.J. Haskal, N.R. Hertzer, C.W. Bakal, M.A. Creager, J.L. Halperin, L.F. Hiratzka, W.R. Murphy, J.W. Olin, J.B. Puschett, K.A. Rosenfield, D. Sacks, J.C. Stanley, L.M. Taylor, C.J. White, J. White, R.A. White, E.M. Antman, S.C. Smith, C.D. Adams, J.L. Anderson, D.P. Faxon, V. Fuster, R.J. Gibbons, S.A. Hunt, A.K. Jacobs, R. Nishimura, J.P. Ornato, R.L. Page, B. Riegel, null, Circulation, 113 (2006) e463-654.
[2] M. Writing Group, T.W. Rooke, A.T. Hirsch, S. Misra, A.N. Sidawy, J.A. Beckman, L.K. Findeiss, J. Golzarian, H.L. Gornik, J.L. Halperin, M.R. Jaff, G.L. Moneta, J.W. Olin, J.C. Stanley, C.J. White, J.V. White, R.E. Zierler, M. Writing Committee, Z.J. Haskal, N.R. Hertzer, C.W. Bakal, M.A. Creager, L.F. Hiratzka, W.R.C. Murphy, J.B. Puschett, K.A. Rosenfield, D. Sacks, L.M. Taylor, R.A. White, M. Accf/Aha Task Force, A.K. Jacobs, J.L. Anderson, N. Albert, S.M. Ettinger, R.A. Guyton, J.S. Hochman, F.G. Kushner, E.M. Ohman, W. Stevenson, C.W. Yancy, Catheterization and Cardiovascular Interventions, 79 (2012) 501-531.
[3] M.A. Cleary, E. Geiger, C. Grady, C. Best, Y. Naito, C. Breuer, Trends in Molecular Medicine, 18 (2012) 394-404.
[4] J.M. Anderson, Annual Review of Materials Research, 31 (2001) 81-110.
[5] B.D. Ratner, S.J. Bryant, Annu. Rev. Biomed. Eng., 6 (2004) 41-75.
[6] S. François, N. Chakfé, B. Durand, G. Laroche, Trends Biomater Artif Organs, 22 (2008) 89-99.
[7] S. François, N. Chakfé, B. Durand, G. Laroche, Acta biomaterialia, 5 (2009) 2418-2428.
[8] O.O. Ige, L.E. Umoru, S. Aribo, ISRN Materials Science, 2012 (2012) 20.
[9] D. Garlotta, Journal of Polymers and the Environment, 9 (2001) 63-84.
[10] J.A. von Fraunhofer, W.J. Sichina, Biomaterials, 13 (1992) 715-720.
[11] S. Nishio, K. Kosuga, K. Igaki, M. Okada, E. Kyo, T. Tsuji, E. Takeuchi, Y. Inuzuka, S. Takeda, T. Hata, Y. Takeuchi, Y. Kawada, T. Harita, J. Seki, S. Akamatsu, S. Hasegawa, N. Bruining, S. Brugaletta, S. de Winter, T. Muramatsu, Y. Onuma, P.W. Serruys, S. Ikeguchi, Circulation, (2012).

[12] I. Uurto, J. Mikkonen, J. Parkkinen, L. Keski-Nisula, T. Nevalainen, M. Kellomäki, P. Törmälä, J.-P. Salenius, Journal of Endovascular Therapy, 12 (2005) 371-379.

[13] C. Deng, Y. Jiang, R. Cheng, F. Meng, Z. Zhong, Nano Today, 7 (2012) 467-480.

[14] R.A. Auras, L.-T. Lim, S.E.M. Selke, H. Tsuji, Poly(lactic Acid): Synthesis, structures, properties, processing, and applications, 2010.

[15] G. Sabbatier, D. Le Nouën, P. Chevallier, B. Durand, G. Laroche, F. Dieval, Polymer Degradation and Stability, 97 (2012) 1520-1526.

[16] S. Ramakrishna, K. Fujihara, W.-E.T. Ma, T.-C. Lim, Z. Ma, An introduction to electrospinning and nanofibers, 2005.

[17] M. Bognitzki, W. Czado, T. Frese, A. Schaper, M. Hellwig, M. Steinhart, A. Greiner, J.H. Wendorff, Advanced Materials, 13 (2001) 70-72.

[18] F. Ko, Y. Gogotsi, A. Ali, N. Naguib, H. Ye, G.L. Yang, C. Li, P. Willis, Advanced Materials, 15 (2003) 1161-1165.

[19] Z. Sun, E. Zussman, A.L. Yarin, J.H. Wendorff, A. Greiner, Advanced Materials, 15 (2003) 1929-1932.

[20] H. Hou, D.H. Reneker, Advanced Materials, 16 (2004) 69-73.

[21] Y. Orlova, N. Magome, L. Liu, Y. Chen, K. Agladze, Biomaterials, 32 (2011) 5615-5624.

[22] S. François, C. Sarra-Bournet, A. Jaffre, N. Chakfé, B. Durand, G. Laroche, Journal of Biomedical Materials Research Part B: Applied Biomaterials, 93B (2010) 531-543.

[23] V. Beachley, X. Wen, Progress in polymer science, 35 (2010) 868-892.

[24] R. Ravichandran, J.R. Venugopal, S. Sundarrajan, S. Mukherjee, S. Ramakrishna, Biomaterials, 33 (2012) 846-855.

[25] N. Naveena, J. Venugopal, R. Rajeswari, S. Sundarrajan, R. Sridhar, M. Shayanti, S. Narayanan, S. Ramakrishna, Journal of Materials Chemistry, 22 (2012) 5239-5253.

[26] C. Arun Richard, J. Venugopal, S. Sundarrajan, S. Ramakrishna, Biomedical Materials, 6 (2011) 015001.

[27] R. Ravichandran, J.R. Venugopal, S. Sundarrajan, S. Mukherjee, S. Ramakrishna, Tissue Engineering Part A, 17 (2011) 1363-1373.

[28] Z. Yin, X. Chen, J.L. Chen, W.L. Shen, T.M. Hieu Nguyen, L. Gao, H.W. Ouyang, Biomaterials, 31 (2010) 2163-2175.

[29] E. Schnell, K. Klinkhammer, S. Balzer, G. Brook, D. Klee, P. Dalton, J. Mey, Biomaterials, 28 (2007) 3012-3025.

[30] K.M. Woo, V.J. Chen, P.X. Ma, Journal of biomedical materials research. Part A, 67 (2003) 531-537.

[31] T.G. Kim, T.A.E.G. Park, Tissue engineering, 12 (2006) 221-233.

[32] J.E. Oliveira, E.A. Moraes, R.G.F. Costa, A.S. Afonso, L.H.C. Mattoso, W.J. Orts, E.S. Medeiros, Journal of Applied Polymer Science, 122 (2011) 3396-3405.

[33] G.E.P. Box, J.S. Hunter, W.G. Hunter, Statistics for experimenters design, innovation and discovery 2nd edition, Wiley Interscience, 2005.

[34] C.J. Ellison, A. Phatak, D.W. Giles, C.W. Macosko, F.S. Bates, Polymer, 48 (2007) 3306-3316.

[35] O. Yordem, M. Papila, Y. Menceloglu, Materials & Design, 29 (2008) 34-44.

[36] R.H. Colby, M. Rubinstein, Macromolecules, 23 (1990) 2753-2757.

[37] M.R. Kasaai, G. Charlet, J. Arul, Food Research International, 33 (2000) 63-67.

[38] Y.P. Neo, S. Ray, A.J. Easteal, M.G. Nikolaidis, S.Y. Quek, Journal of Food Engineering, 109 (2012) 645-651.

[39] P.G. De Gennes, Macromolecules, 9 (1976) 594-598.

[40] A.S. Badami, M.R. Kreke, M.S. Thompson, J.S. Riffle, A.S. Goldstein, Biomaterials, 27 (2006) 596-606.

[41] Y.H. Shih, J.C. Yang, S.H. Li, W.C.V. Yang, C.C. Chen, Textile Research Journal, 82 (2012) 602-612.

[42] H. Tsuji, M. Nakano, M. Hashimoto, K. Takashima, S. Katsura, A. Mizuno, Biomacromolecules, 7 (2006) 3316-3320.

[43] H. Fong, I. Chun, D.H. Reneker, Polymer, 40 (1999) 4585-4592.

[44] R. Inai, M. Kotaki, S. Ramakrishna, Journal of Polymer Science Part B: Polymer Physics, 43 (2005) 3205-3212.

[45] T. Nitanan, P. Opanasopit, P. Akkaramongkolporn, T. Rojanarata, T. Ngawhirunpat, P. Supaphol, Korean J. Chem. Eng., 29 (2012) 173-181.

[46] J.M. Deitzel, J. Kleinmeyer, D. Harris, N.C. Beck Tan, Polymer, 42 (2001) 261-272.

[47] X.M. Mo, C.Y. Xu, M. Kotaki, S. Ramakrishna, Biomaterials, 25 (2004) 1883-1890.

[48] C.P. Barnes, S.A. Sell, E.D. Boland, D.G. Simpson, G.L. Bowlin, Advanced Drug Delivery Reviews, 59 (2007) 1413-1433.

[49] C.S. Kong, S.G. Lee, S.H. Lee, K.H. Lee, H.W. Noh, W.S. Yoo, H.S. Kim, Journal of Macromolecular Science, Part B, 50 (2011) 528-539.

[50] L. Larrondo, R. St. John Manley, Journal of Polymer Science: Polymer Physics Edition, 19 (2003) 933-940.

[51] C.L. Casper, J.S. Stephens, N.G. Tassi, D.B. Chase, J.F. Rabolt, Macromolecules, 37 (2004) 573-578.

[52] P. Gupta, C. Elkins, T.E. Long, G.L. Wilkes, Polymer, 46 (2005) 4799-4810.

[53] L. Kong, G.R. Ziegler, Biomacromolecules, 13 (2012) 2247-2253.

[54] S.L. Shenoy, W.D. Bates, H.L. Frisch, G.E. Wnek, Polymer, 46 (2005) 3372-3384.